Analytical bounds for decoy-state quantum key distribution with discrete phase randomization

Zhaohui Liu, Ahmed Lawey, and Mohsen Razavi

Abstract—We analyze the performance of quantum key distribution (QKD) protocols that rely on discrete phase randomization (DPR). For many QKD protocols that rely on weak coherent pulses (WCPs), continuous phase randomization is assumed, which simplifies the security proofs for such protocols. However, it is challenging to achieve such a perfect phase randomization in practice. As an alternative, we can select a discrete set of global phase values for WCPs, but we need to redo the security analysis for such a source. While security proofs incorporating DPR have been established for several QKD protocols, they often rely on computationally intensive numerical optimizations. To address this issue, in this study, we derive analytical bounds on the secret key generation rate of BB84 and measurementdevice-independent QKD protocols in the DPR setting. Our analytical bounds closely match the results obtained from more cumbersome numerical methods in the regions of interest.

Index Terms—Quantum communication, quantum key distribution, parameter estimation, quantum cryptography.

I. INTRODUCTION

Quantum key distribution (QKD) aims to establish a secure communication channel between two distant parties, conventionally referred to as Alice and Bob. The theoretical security of QKD protocols is based on quantum mechanics [1], [2], as well as a set of assumptions on the behavior and characteristics of the physical devices involved [3]. In real-world scenarios, these assumptions are not necessarily fully met due to a mismatch between the models assumed in the security analysis and that of the actual hardware, leading to potential vulnerabilities [4]–[6]. Consequently, accurate and comprehensive modeling of devices used is essential for conducting realistic security analyses and ensuring the robustness of QKD implementations. In this work, we focus on the specific issue of phase randomization when weak coherent pulses (WCPs) are employed in QKD protocols. In particular, we look at implementations that rely on discrete phase randomization (DPR), as opposed to continuous phase randomization (CPR). While the latter is an easier case to analyze, it would be more practical to establish alignment between the theory and practice in the DPR case.

In many QKD systems, WCPs are widely adopted as a substitute for ideal single-photon sources [7], [8], which require more advanced technology. WCPs, typically generated by attenuated laser sources, offer a practical and scalable solution

This work was supported in part by the UK EPSRC Grants EP/Y037421/1 and EP/X040518/1, and the Doctoral Scholarship offered by School of Electronic and Electrical Engineering at the University of Leeds.

Authors are with School of Electronic and Electrical Engineering, University of Leeds, Leeds LS2 9JT, United Kingdom (e-mail:ml20z8l@leeds.ac.uk; A.Q.Lawey@leeds.ac.uk; M.Razavi@leeds.ac.uk).

due to their ease of generation, cost-effectiveness, and compatibility with existing optical communications infrastructure. A critical aspect of using WCPs securely lies in the application of phase randomization [9]. By using CPR, the output state of the WCP-based encoder can be modeled as a statistical mixture of photon-number (Fock) states, with a Poisson distribution. This transformation is fundamental to the decoy-state method [10], [11], which often enables tight estimation of the single-photon components and protects against certain eavesdropping strategies, such as photon-number-splitting attacks [12], [13]. In the absence of phase randomization, the coherent states retain their phase coherence, invalidating the assumptions underpinning standard security proofs for the decoy state QKD and rendering the system susceptible to sophisticated quantum attacks [14], [15].

Despite its theoretical advantages, achieving ideal CPR in practical OKD systems remains a challenging task. Passive phase randomization techniques that rely on turning the laser sources on and off to generate random global phase values have limitations on the pulse rate because of the transient time needed to stabilize the laser source. Relying on free-running lasers in conjunction with amplitude modulators could also result in correlated phase values for consecutive pulses [16], especially at high repetition rates, again not meeting the required conditions for CPR [4]. On the other hand, active phase randomization schemes, which employ external modulators to impose random phases, presume a uniform distribution of phase values over $[0, 2\pi]$ [5], [17]–[19]. In practice, however, these schemes are constrained by the precision and stability of the modulation hardware, making it challenging to realize full CPR. This discrepancy between theoretical models and practical implementations may introduce subtle vulnerabilities in the security of QKD protocols.

As a pragmatic alternative, DPR has been proposed [20]. In DPR-based implementations, the global phase of each pulse is selected from a finite, predefined set of discrete values. Although, in this approach, we have more control on the phase values used, hence can better ensure the match between theory and implementation, the source model becomes more complicated. Specifically, the resulting quantum channel no longer conforms to the standard photon-number channel model that underpins conventional decoy-state analysis [3], [9], [10], [21]. This deviation invalidates the assumptions used in traditional security proofs [3], necessitating the development of new theoretical frameworks and security analyses tailored to DPR cases.

The challenge of incorporating DPR into QKD protocols has been addressed for both BB84 [20] and measurement-

device-independent (MDI) QKD [22] protocols. However, a significant limitation of existing approaches is related to their parameter estimation, which typically requires solving complex numerical optimization problems. The computational burden of these methods increases substantially with the number of discrete phase slices, making them less practical for real-time implementations, or when there are restrictions on computational power and memory, which is the case in many IoT scenarios [7], [18].

In this work, we present an analytical framework for deriving bounds on the secret key generation rate in both BB84 and MDI QKD protocols in DPR settings. Our approach circumvents the need for computationally intensive numerical optimization by providing closed-form expressions that are easy to calculate. We demonstrate that the analytical bounds closely approximate those obtained through numerical methods, particularly as the number of discrete phase slices increases. Moreover, the proposed analytical techniques are not limited to BB84 and MDI QKD protocols but are also applicable to a broader class of MDI-type protocols that share similar source characteristics. This generality enhances the practicality and adaptability of our methods for real-world QKD deployments.

The structure of this paper is as follows. In Section II, we introduce the theoretical framework, including the distinctions between CPR and DPR, and their implications for BB84 and MDI-QKD protocols. Building on the concepts from [20], we define the optimization problems for parameter estimation and explain the relevant constraints in Section III. Our analytical solutions are then presented in Section IV. In Section V, the numerical and analytical techniques are compared in certain simulation scenarios. Finally, we conclude our paper in Section VI.

II. SYSTEM DESCRIPTION

In this section, we first explain how the source is modeled in the CPR and DPR cases. We then describe BB84 and MDI QKD protocols with DPR in the particular case of vacuum+weak decoy states with phase encoding in X and Y bases [10], [20], [22].

A. Source description

Many QKD protocols employ WCP sources due to their practical feasibility and compatibility with existing optical communications infrastructure. A WCP is characterized by a global phase θ and an average photon number (or intensity) μ , and can be mathematically modeled as the following coherent state:

$$|\sqrt{\mu}e^{i\theta}\rangle = e^{-\frac{\mu}{2}} \sum_{n=0}^{\infty} \frac{\sqrt{\mu}^n e^{in\theta}}{\sqrt{n!}} |n\rangle, \tag{1}$$

where $|n\rangle$, n=0,1,..., represents the Fock state in the optical mode defined by the pulse. In the CPR case, we assume that θ is uniformly distributed in $[0,2\pi)$. The state generated by the WCP source can then be expressed by the following density matrix

$$\frac{1}{2\pi} \int_0^{2\pi} |\sqrt{\mu} e^{i\theta}\rangle \langle \sqrt{\mu} e^{i\theta}| d\theta = e^{-\mu} \sum_{n=0}^{\infty} \frac{\mu^n}{n!} |n\rangle \langle n|, \quad (2)$$

which is diagonal in the Fock basis. This model, known as the photon-number channel, is at the core of many security proofs, particularly those involving WCPs with decoy states [10], [23]. However, realizing perfect phase randomization in practice is technologically demanding. To address this, DPR has been proposed as an alternative.

In DPR, the global phase is uniformly selected from a discrete set of D values, $\theta_j = 2\pi j/D$, where $j = 0, \dots, D-1$, [20]. The source output can then be modeled by the following density matrix

$$\frac{1}{D}\sum_{j=0}^{D-1}|e^{i2\pi j/D}\sqrt{\mu}\rangle\langle e^{i2\pi j/D}\sqrt{\mu}| = \sum_{k=0}^{D-1}p_k^{\mu}|\lambda_k\rangle\langle\lambda_k|, \quad (3)$$

where

$$|\lambda_{k}\rangle = \frac{1}{D\sqrt{p_{k}^{\mu}}} \sum_{j=0}^{D-1} e^{-i2\pi k j/D} |e^{i2\pi j/D}\sqrt{\mu}\rangle$$

$$= \frac{e^{-\frac{\mu}{2}}}{\sqrt{p_{k}^{\mu}}} \sum_{m=0}^{\infty} \frac{\sqrt{\mu}^{mD+k}}{\sqrt{(mD+k)!}} |mD+k\rangle, k = 0, ..., D-1,$$
(4)

and the probability distribution in the DPR case is given by

$$p_k^{\mu} = e^{-\mu} \sum_{m=0}^{\infty} \frac{\mu^{mD+k}}{(mD+k)!},\tag{5}$$

which is a pseudo-Poisson distribution. Eq. (3) shows that the source output is diagonal in $|\lambda_k\rangle$, k=0,...,D-1, rather than number states. When D approaches infinity, the state $|\lambda_k\rangle$ in Eq. (4) approaches the photon-number state $|k\rangle$, and the probability distribution in Eq. (5) will also approach the Poisson distribution.

Next, we describe the two protocols considered in this paper, i.e., BB84 and MDI QKD using DPR.

B. BB84 QKD with DPR

We study the BB84 with the vacuum+weak decoy state protocol using DPR. We consider the phase-encoding implementation of this protocol as shown in Fig. 1. The interferometer at the encoder will generate two pulses, denoted as reference (r) and signal (s), with a phase difference $\{0,\pi\}$ in the X basis, and $\{\pi/2, 3\pi/2\}$ in the Y basis.

In the case of BB84 with DPR, the input state to the encoder for any intensity $\alpha \in \{0, \nu, \mu\}$ is uniformly selected from the set of coherent states $\{|e^{i2\pi j/D}\sqrt{2\alpha}\rangle, j=0,...,D-1\}$. At the receiver, Bob uses a similar Mach-Zehnder interferometer to choose between the X and Y bases, and to measure the phase difference between the reference and signal pulses. After the exchange of the raw key, Alice and Bob follow the typical steps in a QKD protocol to sift and reconcile their keys, and extract a secret key using privacy amplification. We only consider the asymptotic scenario in this work, which means that the intensity μ is the main intensity to be sent and the probability of sending the weak decoy state or the vacuum state is negligibly small. We also use the efficient BB84 protocol [20], where the X basis is primarily used for secret key generation.

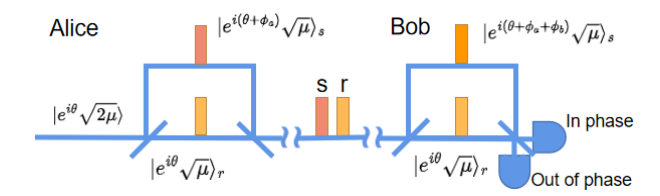


Fig. 1. Schematic for the phase encoding BB84 protocol with DPR. Alice prepares a weak coherent pulse with a randomly chosen discrete phase $\theta \in \{2\pi j/D, j=0,...,D-1\}$. The prepared state is then passed through a Mach-Zehnder interferometer, using which an additional phase shift $\phi_a \in \{0,\pi/2,\pi,3\pi/2\}$ is applied to the signal arm. The resulting pulses are transmitted through a quantum channel to Bob. Upon reception, Bob randomly selects a basis by choosing the relative phase $\phi_b \in \{0,\pi/2\}$ and does the measurement. They will keep the states when one of the two detectors clicks. In the case of double clicks, Bob randomly assigns a bit to his key. Based on the click pattern and their basis choices, Alice and Bob obtain their raw key.

To model the outcome of the encoder in Fig. 1, we use the diagonal format of the phase randomized input state as shown in Eq. (3). For a fixed intensity μ and an encoded input state $|\lambda_k\rangle$, with k=0,...,D-1, the encoder output state in X and Y bases for bits 0 and 1 are given by [20]

$$|0_{x}\rangle_{k} = \sum_{j=0}^{D-1} e^{-i2\pi k j/D} |e^{i2\pi j/D} \sqrt{\mu}\rangle_{r} |e^{i2\pi j/D} \sqrt{\mu}\rangle_{s},$$

$$|1_{x}\rangle_{k} = \sum_{j=0}^{D-1} e^{-i2\pi k j/D} |e^{i2\pi j/D} \sqrt{\mu}\rangle_{r} |e^{i(2\pi j/D + \pi)} \sqrt{\mu}\rangle_{s},$$

$$|0_{y}\rangle_{k} = \sum_{j=0}^{D-1} e^{-i2\pi k j/D} |e^{i2\pi j/D} \sqrt{\mu}\rangle_{r} |e^{i(2\pi j/D + \pi/2)} \sqrt{\mu}\rangle_{s},$$

$$|1_{y}\rangle_{k} = \sum_{j=0}^{D-1} e^{-i2\pi k j/D} |e^{i2\pi j/D} \sqrt{\mu}\rangle_{r} |e^{i(2\pi j/D + 3\pi/2)} \sqrt{\mu}\rangle_{s}.$$
(6)

Here, $|0_x\rangle_k$ and $|1_x\rangle_k$ ($|0_y\rangle_k$ and $|1_y\rangle_k$) are logical qubits in the X (Y) basis for key bits 0 and 1, respectively, and for simplicity, we have not shown the normalization coefficients.

For security purposes, it is essential that Eve cannot distinguish states in X and Y bases. In other words, the density operators for different bases should have an identical expression. This requirement is quantified by the fidelity between the corresponding density matrices [20]:

$$F_{k,\text{BB84}} = \text{tr}\sqrt{\sqrt{\rho_{xk}}\rho_{yk}\sqrt{\rho_{xk}}},\tag{7}$$

where

$$\rho_{xk} = |0_x\rangle_{kk}\langle 0_x| + |1_x\rangle_{kk}\langle 1_x|,$$

$$\rho_{yk} = |0_y\rangle_{kk}\langle 0_y| + |1_y\rangle_{kk}\langle 1_y|.$$
(8)

The numerical results in [20] show that for k=0 and k=1, the fidelity can get close to 1 when D increases, indicating low basis dependence. This behavior is consistent with previous findings and supports the use of these components for key generation [11]. However, for k>1, the fidelity significantly decreases (e.g., around 0.5 for k=2 for parameter values used in [20]), indicating stronger basis dependence. This shows such states do not necessarily contribute much to the secure key rate. Therefore, in this work, we restrict key generation



Fig. 2. Schematic for the phase encoding MDI QKD protocol with DPR. Both Alice and Bob independently prepare weak coherent pulses with randomly chosen discrete phase values $\theta_a,\theta_b\in\{2\pi j/D,j=0,...,D-1\}$. Each prepared state is passed through a Mach-Zehnder interferometer, after which an additional phase shift ϕ_a or ϕ_b is applied to the signal arm to encode the quantum information, where $\phi_a,\phi_b\in\{0,\pi/2,\pi,3\pi/2\}$. The resulting optical pulses are then transmitted through quantum channels to an untrustworthy intermediary, Charlie, who performs an interference measurement on the incoming states. Charlie publicly announces the detection results. Based on this announcement and their own encoding choices, Alice and Bob can post-select correlated events to extract a shared key bit.

to the components with k = 0 and k = 1, where the basis dependence is often sufficiently low under practical conditions.

C. MDI QKD with DPR

Fig. 2 shows the setup for the MDI QKD protocol considered in this paper. As in the case of BB84, we consider the phase encoding implementation of this protocol for the vacuum+weak decoy variant [24]. Alice and Bob each uses a BB84 encoder as explained in Section II-B, hence the output state from each encoder for a $|\lambda_k\rangle$ input is given by Eq. (6). At the midpoint of the quantum channel, a third party, commonly referred to as Charlie, performs an interference measurement on the incoming reference and signal pulses by using singlephoton detectors. A successful detection event is registered when only one of the two detectors clicks for both pairs of reference and signal pulses. Charlie then publicly announces the detection outcomes. Alice and Bob will decide on the shared bit based on the pattern of clicks reported by Charlie [24]. The post-processing steps are followed as described in Section II-B.

To ensure that the bases are mutually unbiased the density operators in the X and Y bases must be identical. This requirement is quantified by the fidelity between the corresponding density matrices [22] as follows:

$$F_{k,\text{MDI}} = \text{tr}\sqrt{\sqrt{\rho_{xk}}\rho_{yk}\sqrt{\rho_{xk}}},\tag{9}$$

where

$$\rho_{xk}$$

$$=(|0_x\rangle_{kk}\langle 0_x|+|1_x\rangle_{kk}\langle 1_x|)_A\otimes(|0_x\rangle_{kk}\langle 0_x|+|1_x\rangle_{kk}\langle 1_x|)_B,$$

$$\rho_{yk}$$

$$=(|0_y\rangle_{kk}\langle 0_y|+|1_y\rangle_{kk}\langle 1_y|)_A\otimes(|0_y\rangle_{kk}\langle 0_y|+|1_y\rangle_{kk}\langle 1_y|)_B.$$
(10)

Again, in practical regimes of operation, it has been observed that the main contribution to the key rate is because of the terms with k=0 or k=1 [22]. Our key rate calculations, in the next section, are, therefore, restricted to such cases.

Box 1: Nonlinear optimization problem for DPR BB84 protocol with vacuum+weak decoy states

Generic Formulation

Minimize

$$R_{\mathrm{BB84}}^{\mathrm{DPR}} = \sum_{k=\{0,1\}} Q_{x,k}^{\mu} [1 - h_2(e_{x,k}^{p,\mu})] - f Q_x^{\mu} h_2(E_x^{\mu}).$$

subject to

$$\begin{split} Q_{\gamma}^{\alpha} &= \sum_{k=0}^{D-1} p_k^{\alpha} Y_{\gamma,k}^{\alpha}, Q_{\gamma}^{\alpha} E_{\gamma}^{\alpha} = \sum_{k=0}^{D-1} p_k^{\alpha} e_{\gamma,k}^{b,\alpha} Y_{\gamma,k}^{\alpha}, \\ |Y_{\gamma,k}^{\alpha_1} - Y_{\gamma,k}^{\alpha_2}| &\leq \epsilon_{\alpha_1 \alpha_2}, |e_{\gamma,k}^{b,\alpha_1} Y_{\gamma,k}^{\alpha_1} - e_{\gamma,k}^{b,\alpha_2} Y_{\gamma,k}^{\alpha_2}| \leq \epsilon_{\alpha_1 \alpha_2}, \\ e_{x,k}^{p,\mu} &\leq e_{y,k}^{b,\mu} + 4 \Delta_k^{\mu} (1 - \Delta_k^{\mu}) (1 - 2 e_{y,k}^{b,\mu}) \\ &+ 4 (1 - 2 \Delta_k^{\mu}) \sqrt{\Delta_k^{\mu} (1 - \Delta_k^{\mu}) e_{y,k}^{b,\mu} (1 - e_{y,k}^{b,\mu})}, \end{split}$$

where $\alpha, \alpha_1, \alpha_2 \in \{0, \nu, \mu\}$, $\gamma = \{x, y\}$ represents X or Y basis, p_k^{μ} is given in Eq. (5), $\epsilon_{\alpha_1 \alpha_2}$ comes from Eq. (13), and Δ_k^{μ} is defined in Eq. (15).

Approximate Formulation

As above, with the additional constraint that $Y_{\gamma,k}^{\alpha} = 0$, for k = 3, 4, ..., D - 1.

III. KEY RATE ANALYSIS

In this section, we review the key rate analysis for the two protocols described in Section II. The corresponding optimization problems are summarized in Box 1 and Box 2, respectively, for BB84 and MDI QKD protocols. Our analytical solutions to these problems are then given in Section IV.

A. BB84 with DPR: Rate analysis

The key rate of the BB84 protocol in Section II-B is lower bounded by [25]

$$R_{\text{BB84}}^{\text{DPR}} = \sum_{k=\{0,1\}} Q_{x,k}^{\mu} [1 - h_2(e_{x,k}^{p,\mu})] - f Q_x^{\mu} h_2(E_x^{\mu}), \quad (11)$$

where $Q_{x,k}^{\mu}$ denotes the gain when Alice encodes the state $|\lambda_k\rangle$ with intensity μ , f is the error correction inefficiency, and $h_2(x) = -x\log_2(x) - (1-x)\log_2(1-x)$ represents the binary Shannon entropy. The term $e_{x,k}^{p,\mu}$ denotes the phase error rate for $|\lambda_k\rangle$ with intensity μ as the input state, which in the X basis corresponds to errors caused by Pauli operator σ_X . The second term in the key rate expression accounts for the cost of error correction, where Q_x^{μ} and E_x^{μ} are the total gain and quantum bit error rate (QBER), respectively, for intensity μ . All above terms are for the X basis, which is the main basis used in the efficient QKD protocol we defined in Section II-B.

To compute the key rate, two critical parameters must be bounded: The yield term $Y^{\mu}_{x,k} = Q^{\mu}_{x,k}/p^{\mu}_k$, and the phase error rate $e^{p,\mu}_{x,k}$. Both parameters are associated with the quantum state $|\lambda_k\rangle$, rather than the photon number state $|k\rangle$ in CPR. Another distinct feature in DPR is that, unlike the CPR case, the yield, gain, and error parameters corresponding to $|\lambda_k\rangle$ are now functions of the employed intensity as well. This will

make the optimization problem more tedious to solve as we see below.

To minimize the lower bound in Eq. (11), we subject it to the following constraints set by the experimental observables:

$$Q_{\gamma}^{0} = Y_{\gamma,0}^{0}, \qquad Q_{\gamma}^{0} E_{\gamma}^{0} = e_{\gamma,0}^{b,0} Y_{\gamma,0}^{0};$$

$$Q_{\gamma}^{\nu} = \sum_{k=0}^{D-1} p_{k}^{\nu} Y_{\gamma,k}^{\nu}, \qquad Q_{\gamma}^{\nu} E_{\gamma}^{\nu} = \sum_{k=0}^{D-1} p_{k}^{\nu} e_{\gamma,k}^{b,\nu} Y_{\gamma,k}^{\nu};$$

$$Q_{\gamma}^{\mu} = \sum_{k=0}^{D-1} p_{k}^{\mu} Y_{\gamma,k}^{\mu}, \qquad Q_{\gamma}^{\mu} E_{\gamma}^{\mu} = \sum_{k=0}^{D-1} p_{k}^{\mu} e_{\gamma,k}^{b,\mu} Y_{\gamma,k}^{\mu}, \qquad (12)$$

where the subscript $\gamma = \{x, y\}$ helps us distinguish between gain, yield, and error terms in basis X and Y, $e_{\gamma,k}^{b,\alpha}$ is the bit error rate when $|\lambda_k\rangle$, with intensity α , is at the encoder input.

To minimize Eq. (11) subject to Eq. (12), we use the following inequalities [20], [25]:

$$|Y_{\gamma,k}^{\alpha_1} - Y_{\gamma,k}^{\alpha_2}| \le \sqrt{1 - F_{\alpha_1 \alpha_2}^2} \equiv \epsilon_{\alpha_1 \alpha_2},$$

$$|e_{\gamma,k}^{b,\alpha_1} Y_{\gamma,k}^{\alpha_1} - e_{\gamma,k}^{b,\alpha_2} Y_{\gamma,k}^{\alpha_2}| \le \sqrt{1 - F_{\alpha_1 \alpha_2}^2} \equiv \epsilon_{\alpha_1 \alpha_2}.$$
(13)

where α_1 and α_2 are two intensity variables in $\{0, \nu, \mu\}$, and the fidelity $F_{\alpha_1\alpha_2}$ is defined as

$$F_{\alpha_1 \alpha_2} = \frac{\sum_{m=0}^{\infty} \frac{(\alpha_1 \alpha_2)^{mD/2}}{(mD)!}}{\sqrt{\sum_{m_1=0}^{\infty} \frac{\alpha_1^{m_1 D}}{(m_1 D)!} \sum_{m_2=0}^{\infty} \frac{\alpha_2^{m_2 D}}{(m_2 D)!}}}.$$
 (14)

Finally, to bound the privacy amplification term, the phase error rate term $e_{x,k}^{p,\mu}$ needs to be upper bounded. We use a virtual protocol described in [25], [26] to establish a relationship between the bit error rate $e_{y,k}^{b,\mu}$ in the Y basis and the phase error rate $e_{x,k}^{p,\mu}$ in the X basis, which characterizes the effective basis dependence in realistic scenarios by the following parameter:

$$\Delta_k^{\mu} = \min(1, \frac{1 - F_{k, \text{BB84}}}{2Y_{r_k}^{\mu}}). \tag{15}$$

Using a bound proved in [11], we can get a relationship between $e^{b,\mu}_{y,k}$ and $e^{p,\mu}_{x,k}$ as follows:

$$\begin{split} e^{p,\mu}_{x,k} &\leq e^{b,\mu}_{y,k} + 4\Delta^{\mu}_{k}(1 - \Delta^{\mu}_{k})(1 - 2e^{b,\mu}_{y,k}) \\ &\quad + 4(1 - 2\Delta^{\mu}_{k})\sqrt{\Delta^{\mu}_{k}(1 - \Delta^{\mu}_{k})e^{b,\mu}_{y,k}(1 - e^{b,\mu}_{y,k})}. \end{split} \tag{16}$$

Putting everything together, in Box 1, we have summarized the generic formulation of the optimization problem that we have to solve. Numerically solving this problem can be cumbersome as $Y_{\gamma,k}^{\alpha}$ terms can be non-negative for all values of k=0,...,D-1. An approximation to this problem can be achieved if we assume $Y_k^{\alpha}=0$ for $k\geq 3$. This is how we find the numerical bounds on the key rate in Section V. In Section IV, however, we derive analytical bounds on the relevant terms in the generic formulation of the key rate optimization problem. It not only reduces the required computational resources, but also its results closely match the results obtained by numerical optimization in the regions of interest.

Box 2: Nonlinear optimization problem for DPR MDI QKD with vacuum+weak decoy states

Generic Formulation

Minimize

$$R_{\rm MDI}^{\rm DPR} = \sum_{k=\{0,1\}} Q_{x,kk}^{\mu\mu} [1 - h_2(e_{x,kk}^{p,\mu\mu})] - f Q_x^{\mu\mu} h_2(E_x^{\mu\mu}). \label{eq:RMDI}$$

subject to

$$\begin{split} Q_{\gamma}^{\alpha\beta} &= \sum_{k,l=0}^{D-1} p_{k}^{\alpha} p_{l}^{\beta} Y_{\gamma,kl}^{\alpha\beta}, \\ Q_{\gamma}^{\alpha\beta} E_{\gamma}^{\alpha\beta} &= \sum_{k,l=0}^{D-1} p_{k}^{\alpha} p_{l}^{\beta} e_{\gamma,kl}^{b,\alpha\beta} Y_{\gamma,kl}^{\alpha\beta}, \\ |Y_{\gamma,kl}^{\alpha_{1}\beta_{1}} - Y_{\gamma,kl}^{\alpha_{2}\beta_{2}}| &\leq \epsilon_{\alpha_{1}\alpha_{2}} + \epsilon_{\beta_{1}\beta_{2}}, \\ |e_{\gamma,kl}^{b,\alpha_{1}\beta_{1}} Y_{\gamma,kl}^{\alpha_{1}\beta_{1}} - e_{\gamma,kl}^{b,\alpha_{2}\beta_{2}} Y_{\gamma,kl}^{\alpha_{2}\beta_{2}}| &\leq \epsilon_{\alpha_{1}\alpha_{2}} + \epsilon_{\beta_{1}\beta_{2}}, \\ e_{x,kk}^{p,\mu\mu} &\leq e_{y,kk}^{b,\mu\mu} + 4\Delta_{kk}^{\mu\mu} (1 - \Delta_{kk}^{\mu\mu}) (1 - 2e_{y,kk}^{b,\mu\mu}), \\ &+ 4(1 - 2\Delta_{kk}^{\mu\mu}) \sqrt{\Delta_{kk}^{\mu\mu} (1 - \Delta_{kk}^{\mu\mu})} e_{y,kk}^{b,\mu\mu} (1 - e_{y,kk}^{b,\mu\mu}), \end{split}$$

where $\alpha, \alpha_1, \alpha_2, \beta, \beta_1, \beta_2 \in \{0, \nu, \mu\}, \gamma = \{x, y\}$ represents either X or Y basis, p_k^{μ} , p_l^{β} are given in Eq. (5), $\epsilon_{\alpha_1\alpha_2}$ and $\epsilon_{\beta_1\beta_2}$ come from Eq. (13), and $\Delta_{kk}^{\mu\mu}$ is defined in Eq. (20).

Approximate Formulation

As above, with the additional constraint that $Y_{\gamma,kl}^{\alpha\beta} = 0$, for k, l = 7, 8, ..., D - 1.

B. MDI QKD with DPR: Rate analysis

Considering the DPR scenario, the secret key rate for the MDI QKD protocol is lower bounded by [22], [25]:

$$R_{\text{MDI}}^{\text{DPR}} = \sum_{k=\{0,1\}} Q_{x,kk}^{\mu\mu} [1 - h_2(e_{x,kk}^{p,\mu\mu})] - f Q_x^{\mu\mu} h_2(E_x^{\mu\mu}), (17)$$

where, in general, $Q_{x,kl}^{\mu\mu}$ and $e_{x,kl}^{p,\mu\mu}$, respectively, are the gain and phase error rate, when Alice and Bob encode $|\lambda_k\rangle$ and $|\lambda_l\rangle$, both with intensity μ , in the X basis, and $Q_x^{\mu\mu}$ and $E_x^{\mu\mu}$ are, respectively, the total gain and QBER when intensity μ is used by both Alice and Bob in the X basis.

First, we note that the following relations hold:

$$Q_{\gamma}^{\alpha\beta} = \sum_{k,l=0}^{D-1} p_k^{\alpha} p_l^{\beta} Y_{\gamma,kl}^{\alpha\beta}, Q_{\gamma}^{\alpha\beta} E_{\gamma}^{\alpha\beta} = \sum_{k,l=0}^{D-1} p_k^{\alpha} p_l^{\beta} e_{\gamma,kl}^{b,\alpha\beta} Y_{\gamma,kl}^{\alpha\beta},$$

$$\tag{18}$$

where $\gamma = \{x, y\}$ represents X or Y basis, and $Q_{\gamma}^{\alpha\beta}$ and $E_{\gamma}^{\alpha\beta}$ are experimentally observable variables in basis γ , respectively, representing the total gain and QBER, when Alice and Bob use intensities α and β . The term $Y_{\gamma,kl}^{\alpha\beta}$ denotes the yield in basis γ when Alice and Bob encode the states $|\lambda_k\rangle$, with intensity α , and $|\lambda_l\rangle$, with intensity β , respectively, and $e_{\gamma,kl}^{b,\alpha\beta}$ is the corresponding bit error rate.

Similar to Eq. (13), in the MDI case, we have the following relationships [20]:

$$|Y_{\gamma,kl}^{\alpha_1\beta_1} - Y_{\gamma,kl}^{\alpha_2\beta_2}| \le \epsilon_{\alpha_1\alpha_2} + \epsilon_{\beta_1\beta_2},$$

$$|e_{\gamma,kl}^{b,\alpha_1\beta_1} Y_{\gamma,kl}^{\alpha_1\beta_1} - e_{\gamma,kl}^{b,\alpha_2\beta_2} Y_{\gamma,kl}^{\beta_2}| \le \epsilon_{\alpha_1\alpha_2} + \epsilon_{\beta_1\beta_2}.$$
(19)

The final step is to bound the phase error rate $e_{x,kk}^{p,\mu\mu}$ in the X basis by the bit error rate $e^{b,\mu\mu}_{y,kk}$ in the Y basis. Similar to what we did in Section III-A, the basis dependence can be characterized by [25], [26]:

$$\Delta_{kk}^{\mu\mu} = \min(1, \frac{1 - F_{k,\text{MDI}}}{2Y_{x,kk}^{\mu\mu}}),\tag{20}$$

which corresponds to the case when both Alice and Bob encode $|\lambda_k\rangle$. Thereby, in our optimization problem, we only consider the contribution from $e_{x,kk}^{p,\mu}$ for k=0 and k=1, for which the following upper bound is given [11], [22], [27]:

$$\begin{split} e^{p,\mu\mu}_{x,kk} \leq & e^{b,\mu\mu}_{y,kk} + 4\Delta^{\mu\mu}_{kk}(1-\Delta^{\mu\mu}_{kk})(1-2e^{b,\mu\mu}_{y,kk}) \\ & + 4(1-2\Delta^{\mu\mu}_{kk})\sqrt{\Delta^{\mu\mu}_{kk}(1-\Delta^{\mu\mu}_{kk})e^{b,\mu\mu}_{y,kk}(1-e^{b,\mu\mu}_{y,kk})}. \end{split} \tag{21}$$

Finally, we can construct the numerical optimization problem in Box 2 to work out the key rate of DPR MDI QKD protocol. The approximate formulation used for numerically solving this problem is also shown in Box 2. The analytical methods are discussed in Section IV-B and Appendix B.

IV. ANALYTICAL BOUNDS

In this section, we present analytical bounds on the key parameters in Eq. (11) and Eq. (17). The key objective is to derive bounds on such parameters using experimentally accessible observables from vacuum, decoy, and signal states. Our approach parallels the methodology used in CPR QKD [10], [21], [28], but requires additional care due to the differences introduced by DPR [22]. Here, we summarize the final results leaving detailed derivations to Appendix A and Appendix B.

A. Analytical bounds for BB84 with DPR

In this section, we give analytical bounds on $Y^{\mu}_{\gamma,0}, Y^{\mu}_{\gamma,1}$ $W_{y,0}^{\mu}$, and $W_{y,1}^{\mu}$ that contribute to the key rate expression in Eq. (11), $W_{\gamma,k}^{\alpha}=e_{\gamma,k}^{b,\alpha}Y_{\gamma,k}^{\alpha}$. First, note that $Q_{\gamma}^{0}=Y_{\gamma,0}^{0}$ and $Q_{\gamma}^{0}E_{\gamma}^{0}=W_{\gamma,0}^{0}$. Using

Eq. (13), we have

$$Y_{\gamma,0}^{\mu} \ge Y_{\gamma,0}^{\mu L} \equiv \max(Q_{\gamma}^{0} - \epsilon_{\mu 0}, 0),$$

$$W_{y,0}^{\mu} \le W_{y,0}^{\mu U} \equiv \min(Q_{y}^{0} E_{y}^{0} + \epsilon_{\mu 0}, 0.5),$$
(22)

where Q_{γ}^{0} and $Q_{y}^{0}E_{y}^{0}$ are directly obtained from observables. Using these, we can derive an upper bound for the bit error rate as $e^{b,\mu}_{y,0} \leq e^{b,\mu U}_{y,0} \equiv W^{\mu U}_{y,0}/Y^{\mu L}_{y,0}$.

The next key parameters in the analysis are $Y_{\gamma,1}^{\mu}$ and $W_{y,1}^{\mu} =$ $e_{y,1}^{b,\mu}Y_{y,1}^{\mu}$, which correspond to the state $|\lambda_1\rangle$. The lower bound on $Y_{\gamma,1}^{\mu}$ is given by:

$$\begin{split} &Y_{\gamma,1}^{\mu} \geq Y_{\gamma,1}^{\mu L} \\ &\equiv \frac{e^{\alpha_{1}}Q_{\gamma}^{\alpha_{1}} - e^{\alpha_{2}}Q_{\gamma}^{\alpha_{2}} - (e^{\alpha_{1}}p_{0}^{\alpha_{1}} - e^{\alpha_{2}}p_{0}^{\alpha_{2}} - A_{\alpha_{1}\alpha_{2}}e^{\mu}p_{0}^{\mu})Q_{\gamma}^{0}}{(e^{\alpha_{1}}p_{1}^{\alpha_{1}} - e^{\alpha_{2}}p_{1}^{\alpha_{2}} - A_{\alpha_{1}\alpha_{2}}e^{\mu}p_{1}^{\mu})} \\ &- \frac{A_{\alpha_{1}\alpha_{2}}e^{\mu}Q^{\mu} + A_{\alpha_{1}\alpha_{2}}e^{\mu}p_{0}^{\mu}\epsilon_{\mu 0} + e^{\alpha_{1}}p_{0}^{\alpha_{1}}\epsilon_{\alpha_{1}0} + e^{\alpha_{2}}p_{0}^{\alpha_{2}}\epsilon_{\alpha_{2}0}}{(e^{\alpha_{1}}p_{1}^{\alpha_{1}} - e^{\alpha_{2}}p_{1}^{\alpha_{2}} - A_{\alpha_{1}\alpha_{2}}e^{\mu}p_{1}^{\mu})} \\ &- \frac{(e^{\alpha_{1}} - e^{\alpha_{1}}p_{0}^{\alpha_{1}})\epsilon_{\mu\alpha_{1}} + (e^{\alpha_{2}} - e^{\alpha_{2}}p_{0}^{\alpha_{2}})\epsilon_{\mu\alpha_{2}}}{(e^{\alpha_{1}}p_{1}^{\alpha_{1}} - e^{\alpha_{2}}p_{1}^{\alpha_{2}} - A_{\alpha_{1}\alpha_{2}}e^{\mu}p_{1}^{\mu})}, \end{split} \tag{23}$$

where

$$A_{\alpha_1 \alpha_2} = \max_{k \ge 2} \left\{ \frac{e^{\alpha_1} p_k^{\alpha_1} - e^{\alpha_2} p_k^{\alpha_2}}{e^{\mu} p_k^{\mu}} \right\}, \tag{24}$$

and we set $\alpha_1 = \nu$ and $\alpha_2 = 0$, because they often give the best results. In Eq. (24), we can prove that $A_{\alpha_1\alpha_2}$ is monotonically decreasing with k when $\alpha_1 > \alpha_2$ and achieves its maximal value at k = 2. The above formulation nevertheless gives us the option to explore alternative combinations of α_1 and α_2 without compromising the security of the protocol.

Next, the upper bound on $W_{u,1}^{\mu}$ is given by

$$\begin{split} W_{y,1}^{\mu} &\leq W_{y,1}^{\mu U} \\ &\equiv \frac{e^{\alpha_{1}}Q_{y}^{\alpha_{1}}E_{y}^{\alpha_{1}} - e^{\alpha_{2}}Q_{y}^{\alpha_{2}}E_{y}^{\alpha_{2}} - (e^{\alpha_{1}}p_{0}^{\alpha_{1}} - e^{\alpha_{2}}p_{0}^{\alpha_{2}})Q_{y}^{0}E_{y}^{0}}{e^{\alpha_{1}}p_{1}^{\alpha_{1}} - e^{\alpha_{2}}p_{1}^{\alpha_{2}}} \\ &+ \frac{e^{\alpha_{1}}p_{0}^{\alpha_{1}}\epsilon_{\alpha_{1}0} + e^{\alpha_{2}}p_{0}^{\alpha_{2}}\epsilon_{\alpha_{2}0} + e^{\alpha_{1}}p_{1}^{\alpha_{1}}\epsilon_{\mu\alpha_{1}} + e^{\alpha_{2}}p_{1}^{\alpha_{2}}\epsilon_{\mu\alpha_{2}}}{e^{\alpha_{1}}p_{1}^{\alpha_{1}} - e^{\alpha_{2}}p_{1}^{\alpha_{2}}}, \end{split}$$

where the condition $e^{\alpha_1}p_1^{\alpha_1} - e^{\alpha_2}p_1^{\alpha_2} > 0$ is met when $\alpha_1 >$ α_2 , which is the case for our choice of $\alpha_1 = \nu$ and $\alpha_2 = 0$. Consequently, the upper bound of the bit error rate is $e_{y,1}^{b,\mu U} =$ $W_{y,1}^{\mu U}/Y_{y,1}^{\mu L}$.

In summary, by employing the vacuum+weak decoy state method and applying fidelity-based constraints, we are able to derive lower bounds for the yields $Y^{\mu}_{\gamma,0}$ and $Y^{\mu}_{\gamma,1}$, as shown in Eq. (22) and Eq. (23), respectively. Similarly, upper bounds for the bit error rates $e_{y,0}^{b,\mu}$ and $e_{y,1}^{b,\mu}$ are obtained by using Eq. (22) and Eq. (25). With these bounds, the lower bound on the key rate can be calculated by using Eq. (11), where the phase error rate of the X basis is bounded via the bit error rate in the Y basis, as described in Eq. (16). All other required parameters in Eq. (11) are either directly measurable in experiments or computable through simulations.

B. Analytical bounds for MDI QKD with DPR

In the DPR case, a lower bound on the key rate of the MDI-QKD protocol is given by Eq. (17). The variables we need to bound are $Y_{\gamma,kk}^{\mu\mu} = Q_{\gamma,kk}^{\mu\mu}/(p_k^\mu p_k^\mu)$ and $e_{y,kk}^{b,\mu\mu}$, for $k \in \{0,1\}$, from which $e_{x,kk}^{p,\mu\mu}$ can be bound.

The bounds for variables related to $|\lambda_{00}\rangle$ are expressed as follows:

$$Y_{\gamma,00}^{\mu\mu} \ge Y_{\gamma,00}^{\mu\mu L} \equiv \max(Q_{\gamma}^{00} - 2\epsilon_{\mu 0}, 0),$$

$$W_{y,00}^{\mu\mu} \le W_{y,00}^{\mu\mu U} \equiv \max(Q_{y}^{00} E_{y}^{00} + 2\epsilon_{\mu 0}, 0.5),$$
 (26)

where Q_y^{00} and $Q_y^{00}E_y^{00}$ are observables, and $W_{\gamma,k}^{\alpha\beta}=e_{\gamma,k}^{b,\alpha\beta}Y_{\gamma,k}^{\alpha\beta}$. An upper bound for the bit error rate is $e_{y,00}^{b,\mu\mu}\leq e_{y,00}^{b,\mu\mu U}=W_{y,00}^{\mu\mu U}/Y_{y,00}^{\mu\mu L}$. In terms of bounds on $Y_{\gamma,11}^{\mu\mu}$ and $W_{y,11}^{\mu\mu}$, we use Eq. (19)

and some mathematical inequalities in Appendix B to obtain

$$Y_{\gamma,11}^{\mu\mu} \ge Y_{\gamma,11}^{\mu\mu L} \equiv \frac{e^{\alpha+\beta}Q_{\gamma}^{\alpha\beta} - T_1 - GT_s - \epsilon_{\bar{s}} - 2G\epsilon_{T_s} - \epsilon_s}{e^{\alpha+\beta}p_1^{\alpha}p_1^{\beta} - G(e^{\mu}p_1^{\mu})^2},$$
(27)

where

$$T_{1} = e^{\alpha+\beta} (p_{0}^{\alpha} Q_{\gamma}^{0\beta} + p_{0}^{\beta} Q_{\gamma}^{\alpha 0} - p_{0}^{\alpha} p_{0}^{\beta} Q_{\gamma}^{00}) \quad \text{and}$$

$$T_{s} = e^{2\mu} (Q_{\gamma}^{\mu\mu} - p_{0}^{\mu} (Q_{\gamma}^{0\mu} + Q_{\gamma}^{\mu 0}) + p_{0}^{\mu} p_{0}^{\mu} Q_{\gamma}^{00})$$
 (28)

can be calculated from observed values; G is given by $\max(A, B, C)$, where

$$A = \max_{k \ge 2} \left\{ \frac{e^{\alpha + \beta} p_k^{\alpha} p_1^{\beta}}{e^{2\mu} p_k^{\mu} p_1^{\mu}} \right\}, \quad B = \max_{l \ge 2} \left\{ \frac{e^{\alpha + \beta} p_1^{\alpha} p_l^{\beta}}{e^{2\mu} p_1^{\mu} p_l^{\mu}} \right\},$$

$$C = \max_{k,l \ge 2} \left\{ \frac{e^{\alpha + \beta} p_k^{\alpha} p_l^{\beta}}{e^{2\mu} p_k^{\mu} p_l^{\mu}} \right\}.$$
(29)

Here, A, B, and C are monotonically decreasing with respect to k and l and achieve their maximal values at k = l = 2. Also, from Eq. (19), we show in Appendix B that

$$\epsilon_{\bar{s}} = e^{\alpha + \beta} (p_0^{\alpha} + p_0^{\alpha} p_0^{\beta}) \epsilon_{\alpha 0} + e^{\alpha + \beta} (p_0^{\beta} + p_0^{\alpha} p_0^{\beta}) \epsilon_{\beta 0}$$

$$+ e^{\alpha + \beta} p_1^{\alpha} p_1^{\beta} (\epsilon_{\alpha \mu} + \epsilon_{\beta \mu}),$$

$$\epsilon_{s} = e^{\alpha + \beta} (\sum_{a=2}^{N-1} p_a^{\alpha} p_1^{\beta} (\epsilon_{\alpha \mu} + \epsilon_{\beta \mu}) + \sum_{b=2}^{N-1} p_1^{\alpha} p_b^{\beta} (\epsilon_{\alpha \mu} + \epsilon_{\beta \mu})$$

$$+ \sum_{a=2}^{N-1} \sum_{b=2}^{N-1} p_a^{\alpha} p_b^{\beta} (\epsilon_{\alpha \mu} + \epsilon_{\beta \mu})),$$

$$\epsilon_{T_s} = e^{2\mu} (p_0^{\mu} + p_0^{\mu} p_0^{\mu}) \epsilon_{\mu 0}.$$
(30)

One important condition is $e^{\alpha+\beta}p_1^{\alpha}p_1^{\beta}-G(e^{\mu}p_1^{\mu})^2>0$ to let the value of $Y_{\gamma,11}^{\mu\mu L}$ be positive and meaningful. After calculation, we can prove that as long as α and β are not both equal to μ , this condition holds, which is the reason why decoy states must be involved in the analytical methods. As a result, in this work, we use $\alpha = \beta = \nu$ to analyze the key rate.

Next, the upper bound on $W_{v,11}^{\mu\mu}$ is calculated from

$$W_{y,11}^{\mu\mu} \le W_{y,11}^{\mu\mu U} = \frac{e^{\alpha+\beta} Q_y^{\alpha\beta} E_y^{\alpha\beta} - T_2 - \epsilon_{\bar{s}}}{e^{\alpha+\beta} p_1^{\alpha} p_1^{\beta}}, \quad (31)$$

where

$$T_2 = e^{\alpha+\beta} (p_0^{\alpha} Q_y^{0\beta} E_y^{0\beta} + p_0^{\beta} Q_y^{\alpha 0} E_y^{\alpha 0} - p_0^{\alpha} p_0^{\beta} Q_y^{00} E_y^{00}).$$
 (32)

V. SIMULATION RESULTS AND DISCUSSION

In our simulations, we consider the scenario in which no eavesdropper (Eve) is present, but system parameters and imperfections determine the observed values in an experiment. In our simulations of the BB84 protocol, the total gain and

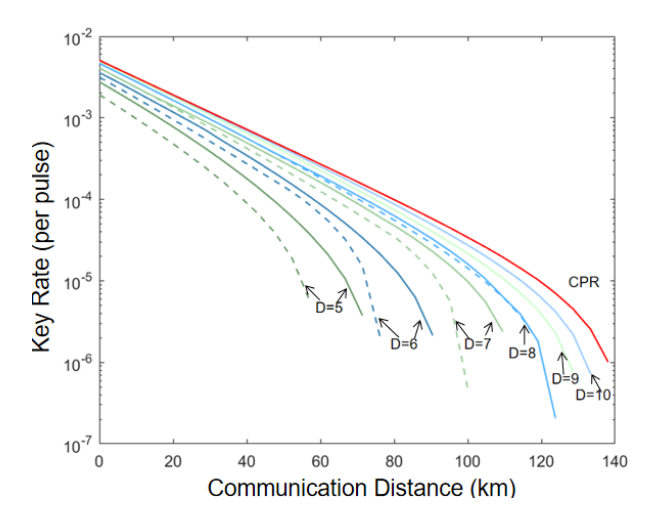


Fig. 3. Secret key generation rates for the DPR BB84 protocol using numerical (solid lines) and analytical (dashed) methods. The mean number of photons for the signal and decoy states are optimized to get the maximum key rate. The best performing curve is based on the vacuum+weak decoy states and CPR. The remaining curves are generated when considering D phase slices and vacuum+weak decoy states. The simulation parameters are shown in Table I [20], [28].

TABLE I
PARAMETER VALUES USED IN SIMULATIONS

Detection Efficiency	0.045
Dark Count Rate Per Pulse, p_d	1.7×10^{-6}
Error Correction Inefficiency, f	1.16
Phase Misalignment Error Rate, e_d	0.033
Loss Factor	0.21 dB/km

the corresponding QBER, for an intensity α , are, respectively, assumed to be [10], [20], [29]

$$Q_{\gamma}^{\alpha} = Y_0 + 1 - e^{-\eta \alpha},$$

$$Q_{\gamma}^{\alpha} E_{\gamma}^{\alpha} = e_0 Q_{\gamma}^{\alpha} - (e_0 - e_d)(1 - e^{-\eta \alpha})(1 - p_d),$$
 (33)

where $Y_0=2p_d$ denotes the vacuum yield, p_d is the dark count rate per pulse, η represents the overall channel transmittance, $e_0=0.5$ is the error rate associated with vacuum states, and e_d denotes the phase misalignment error rate. In our simulations of the MDI QKD protocol, the total gain and the corresponding QBER when Alice sends states with intensity α and Bob sends states with intensity β are, respectively, taken as [22], [30]

$$Q_{\gamma}^{\alpha\beta} = (Y_{00} + 1 - e^{-\eta\alpha})(Y_{00} + 1 - e^{-\eta\beta}),$$

$$Q_{\gamma}^{\alpha\beta} E_{\gamma}^{\alpha\beta} = Y_{00}(Y_{00} + 2 - e^{-\eta\alpha} - e^{-\eta\beta})/2$$

$$+ e_d(1 - e^{-\eta\alpha})(1 - e^{-\eta\beta}), \tag{34}$$

where Y_{00} is assumed to be $2p_d$. Using the above values as our observables, we can use the techniques introduced in Section III and Section IV to bound the key rate.

Figure 3 presents the secret key rates for the vacuum+weak decoy BB84 protocol, using the numerical method (solid lines) described in Section III-A, by solving the optimization problem in Box 1, Approximate Formulation, and the analytical method (dashed lines) outlined in Section IV-A. The corresponding bit error rates are shown in Fig. 4. The simulation parameters are shown in Table I [20], [28]. During

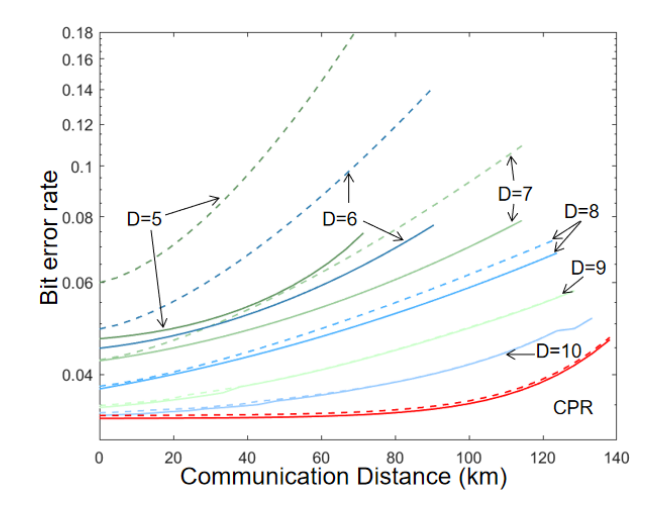


Fig. 4. Bit error rate $e^{b,\mu}_{y,1}$ for the DPR BB84 protocol using numerical (solid) and analytical (dashed) methods. Results for the CPR case are shown as well. For clarity, the curves corresponding to D<9 are smoothed to better display the relationship between the bit error rate and either the phase slice number or the communication distance.

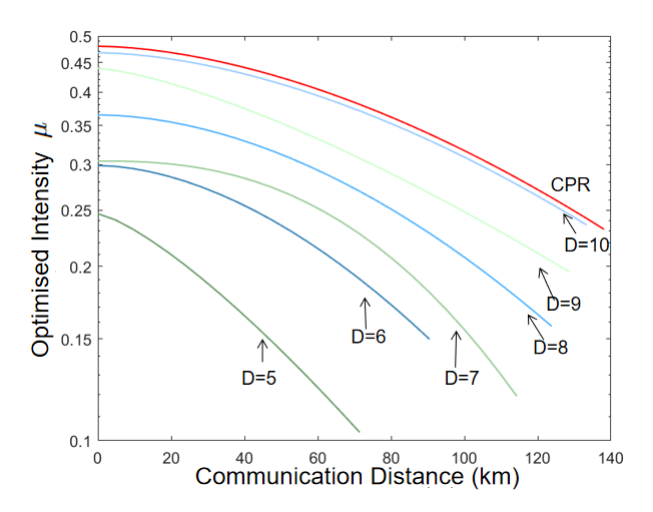


Fig. 5. The optimized value of μ for different number of phase slices ranging from D=5 to D=10, versus distance in the DPR BB84 protocol. A CPR related curve is provided for comparison. Only the numerical results are given here because we get almost the same value of optimized μ from both methods. All curves are smoothed to mask numerical fluctuations.

the optimization process for both numerical and analytical methods, the intensity μ is varied within the range [0,0.5], and the decoy intensity ν within [0,0.02], to optimize the key rate. The optimized values of μ are displayed in Fig. 5. It is worth noting that some curves in Fig. 4 and Fig. 5 have been smoothed, using function fitting, to reduce numerical fluctuations and to better visualize the trends in bit error rates and intensities μ under different conditions.

As shown in Fig. 3, our analytical key rates exhibit increasing accuracy with larger values of the phase slice parameter D when compared with numerical results. When D > 7, the analytical results become nearly indistinguishable from those obtained via numerical optimization, indicating that the analytical approximation is sufficiently tight in this regime. This is because when D increases, we get closer to the CPR

case, where there is little difference between numerical and analytical results. Conversely, for smaller values of D, the protocol remains functional but achieves secure key exchange only over shorter distances, highlighting the trade-off between implementation simplicity and performance, due to looser bounds on some parameters, such as $e_{y,1}^{b,\mu}$ shown in Fig. 4.

The bit error rate results presented in Fig. 4 help explain the observed differences in key rate performance. The bit error rate $e_{y,1}^{b,\mu}$ determines the bound on $e_{x,1}^{p,\mu}$ in the key rate in Eq. (11), and itself is bounded via Eq. (13). From Eq. (14), we find that the fidelity $F_{\nu 0}$ decreases as D decreases, leading to a looser bound in Eq. (13). Although both methods use the same constraint, numerical methods optimize over the entire range of variables while analytical methods directly pick the worst case for some individual variables, which leads to looser upper bounds in the analytical methods than in the numerical results. For sufficiently large values of D, the analytical bounds closely follow the numerical bounds across the entire communication distance. However, as the number of phase slices decreases, the error rates increase rapidly, and the gap between the analytical and numerical bounds becomes more pronounced. This behavior highlights the impact of phase slice resolution on the accuracy of the analytical estimation.

The performance of the DPR BB84 protocol is also closely tied to the choice of signal intensity μ , which directly influences both the secret key rate and the bit error rate. In Fig. 5, when the number of phase slices is D = 10, the optimized intensity μ , obtained through numerical methods, starts at approximately 0.47. This value is consistent with the findings in [20], where a typical signal intensity of $\mu = 0.5$ was reported. As the number of phase slices decreases or the communication distance increases, the optimized μ correspondingly decreases in order to maintain a positive secret key rate. This behavior can be explained as follows. When D is small, the phase-randomized states become more distinguishable, which compromises the fidelity between the prepared states. To ensure the fidelity in Eq. (7) remains high, we must reduce μ ; otherwise, the estimation of the phase error rate $e_{x,1}^{p,\mu}$ in Eq. (16) becomes unreliable. Similarly, at longer communication distances, the channel loss increases significantly, which leads to greater information leakage or error correction cost, quantified by the term $fQ^{\mu}_{\pi}h_{2}(E^{\mu}_{\pi})$ in Eq. (11). To mitigate this, the system must again reduce μ , both to suppress multi-photon emissions and to preserve a positive key rate under adverse channel conditions.

Figure 6 shows the secret key generation rates for the DPR MDI QKD using the vacuum+weak decoy state technique. The corresponding bit error rates are shown in Fig. 7 and the trend of the optimized μ is depicted in Fig. 8. The key rates are computed using two approaches: the numerical optimization method presented in Section III-B, Box 2, Approximate Formulation (solid lines), and our analytically derived solutions described in Section IV-B (dashed lines). The simulation parameters are shown in Table I. To determine the optimal key rate, we optimize the intensity μ within the range [0,0.4] and the decoy intensity ν within [0,0.02]. It is worth noting that some curves in Fig. 7 and Fig. 8 have been smoothed, using function fitting, to better visualize the trends

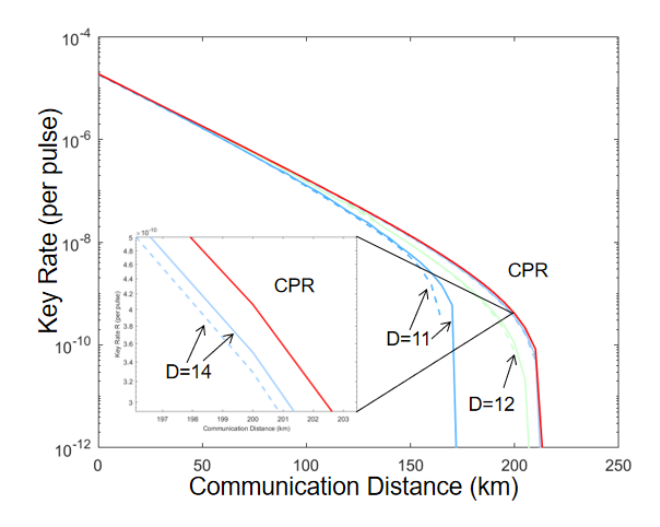


Fig. 6. Secret key generation rates for the MDI-QKD protocol using numerical (solid lines) and analytical (dashed) methods. The mean number of photons for the signal and decoy states are optimized to get the maximum key rate. The best performing curve is based on the vacuum+weak decoy states and CPR. The remaining curves are generated when considering *D* phase slices and vacuum+weak decoy states. The parameters used are give in Table I [22], [28].

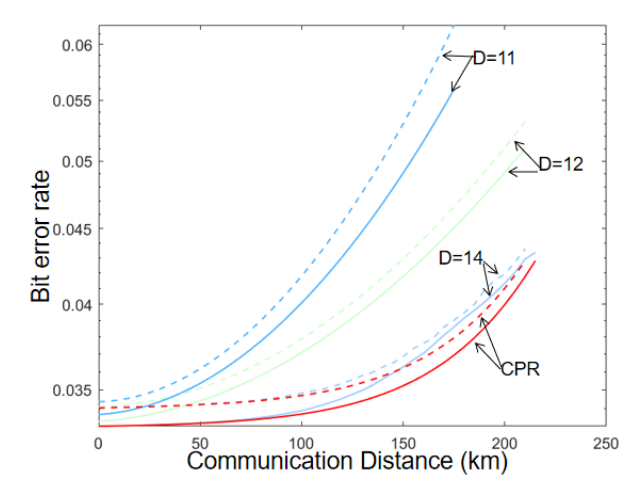


Fig. 7. Bit error rate, $e_{y,1}^{b,\mu\mu}$, for the DPR MDI QKD protocol using numerical (solid) and analytical (dashed) methods. Results for the CPR case are shown as well. For clarity, the curves corresponding to D<14 are smoothed to better display the relationship between the bit error rate and either the phase slice number or the communication distance.

of bit error rates and intensity μ under different conditions.

As shown in Fig. 6, once the number of discrete phases D reaches 14, the performance gap between the DPR protocol and the fully randomized case becomes negligible, which is consistent with the result in [22]. Our analytical solutions exhibit strong agreement with the numerically optimized results for both the CPR and DPR cases with phase slice numbers D>10. Although numerical optimization provides accurate performance estimates, it is computationally intensive and may hinder real-time parameter estimation. In contrast, our analytical bounds offer a fast and practical alternative for determining system parameters and the required level of privacy amplification.

Fig. 7 shows that our analytical bit error rate results closely

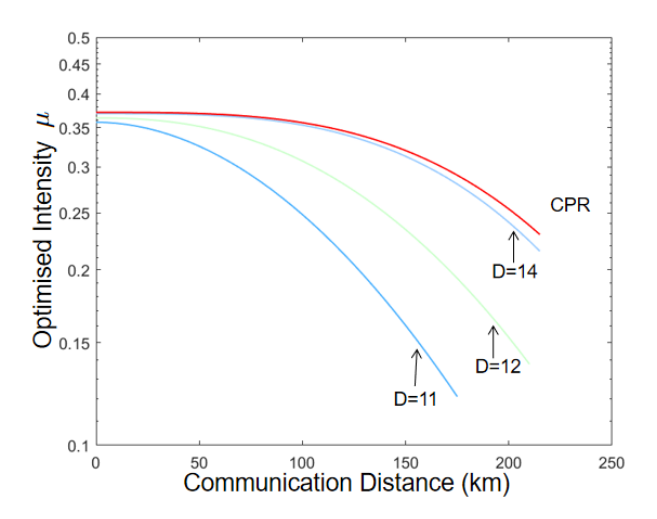


Fig. 8. The optimum intensity μ for different values of D versus distance in the DPR MDI QKD protocol. All curves are smoothed to mask numerical fluctuations.

match the numerical ones. The discrepancy observed at 0 km is attributed to the formulation in Eq. (19), where two ϵ parameters are introduced during the variable transformation. Although both methods are subject to the same constraints, analytical bounds always select the worst-case value for each variable independently. In contrast, numerical bounds can become tight when the full set of variables is jointly considered. This discrepancy leads to an initial mismatch.

We also compare the optimized μ with respect to different phase slices and communication distances in Fig. 8. As shown in Fig. 8, the maximum value of the optimized signal intensity μ is approximately 0.37 in the CPR case. This value gradually decreases as the number of phase slices is reduced or as the communication distance increases, which is caused by the same reason as we discussed in Fig. 5.

VI. SUMMARY

In this work, we presented an analytical framework for evaluating the performance of QKD protocols based on discrete-phase randomization (DPR). Existing DPR-based security proofs often rely on computationally intensive numerical optimization [20], [22], which limits their practicality in real-time or resource-constrained environments. We derived analytical bounds for the secret key rates of BB84 and MDI QKD protocols under DPR. These bounds closely matched numerical results and significantly reduced processing time, particularly when the number of phase slices was sufficiently large. The proposed methods substantially reduce computational overhead and are applicable to other MDI-type protocols.

Future work may extend this framework to finite-key analysis. Preliminary studies on DPR BB84 and twin-field (TF) QKD [18], [31] use semidefinite programming to obtain numerical bounds. Our analytical approach could make such analysis more tractable. Additionally, the mode-pairing QKD protocol [32], a promising member of the MDI QKD family, merits further investigation due to its improved implementation feasibility compared to TF QKD [33].

ACKNOWLEDGMENTS

The authors would like to thank M. Ghalaii, L. Wooltorton, G. Currás Lorenzo and X. Sixto for enlightening discussions.

APPENDIX A ANALYTICAL BB84 BOUNDS

In this appendix, we derive Eq. (23) and Eq. (25) in the main text. We use γ to represent either X or Y basis.

First, we can rewrite Q^{α}_{γ} and $Q^{\alpha}_{\gamma}E^{\alpha}_{\gamma}$ as [10]

$$e^{\alpha}Q_{\gamma}^{\alpha} = e^{\alpha} \sum_{k=0}^{D-1} p_k^{\alpha} Y_{\gamma,k}^{\alpha},$$

$$e^{\alpha}Q_{\gamma}^{\alpha} E_{\gamma}^{\alpha} = e^{\alpha} \sum_{k=0}^{D-1} p_k^{\alpha} W_{\gamma,k}^{\alpha},$$
(35)

where $e^{\alpha} = \exp(\alpha)$. To bound $Y^{\mu}_{\gamma,1}$, we use the above gain equations for two different intensity values, $\alpha_1 > \alpha_2$, to obtain

$$\begin{split} &e^{\alpha_1}Q_{\gamma}^{\alpha_1}-e^{\alpha_2}Q_{\gamma}^{\alpha_2}\\ &=e^{\alpha_1}p_0^{\alpha_1}Y_{\gamma,0}^{\alpha_1}-e^{\alpha_2}p_0^{\alpha_2}Y_{\gamma,0}^{\alpha_2}+e^{\alpha_1}p_1^{\alpha_1}Y_{\gamma,1}^{\alpha_1}-e^{\alpha_2}p_1^{\alpha_2}Y_{\gamma,1}^{\alpha_2}\\ &+\sum_{k=2}^{D-1}(e^{\alpha_1}p_k^{\alpha_1}Y_{\gamma,k}^{\alpha_1}-e^{\alpha_2}p_k^{\alpha_2}Y_{\gamma,k}^{\alpha_2})\\ &\leq (e^{\alpha_1}p_0^{\alpha_1}-e^{\alpha_2}p_0^{\alpha_2})Y_{\gamma,0}^0+e^{\alpha_1}p_0^{\alpha_1}\epsilon_{\alpha_10}+e^{\alpha_2}p_0^{\alpha_2}\epsilon_{\alpha_20}\\ &+(e^{\alpha_1}p_1^{\alpha_1}-e^{\alpha_2}p_1^{\alpha_2})Y_{\gamma,1}^\mu+e^{\alpha_1}p_1^{\alpha_1}\epsilon_{\mu\alpha_1}+e^{\alpha_2}p_1^{\alpha_2}\epsilon_{\mu\alpha_2}\\ &+\sum_{k=2}^{D-1}[(e^{\alpha_1}p_k^{\alpha_1}-e^{\alpha_2}p_k^{\alpha_2})Y_{\gamma,k}^\mu+e^{\alpha_1}p_k^{\alpha_1}\epsilon_{\mu\alpha_1}+e^{\alpha_2}p_k^{\alpha_2}\epsilon_{\mu\alpha_2}]\\ &\leq (e^{\alpha_1}p_0^{\alpha_1}-e^{\alpha_2}p_0^{\alpha_2})Q_{\gamma}^0+(e^{\alpha_1}p_1^{\alpha_1}-e^{\alpha_2}p_1^{\alpha_2})Y_{\gamma,1}^\mu\\ &+A_{\alpha_1\alpha_2}\sum_{k=2}^{D-1}[e^\mu p_k^\mu Y_{\gamma,k}^\mu+\frac{1}{A_{\alpha_1\alpha_2}}(e^{\alpha_1}p_k^{\alpha_1}\epsilon_{\mu\alpha_1}+e^{\alpha_2}p_k^{\alpha_2}\epsilon_{\mu\alpha_2})]\\ &+e^{\alpha_1}p_0^{\alpha_1}\epsilon_{\alpha_10}+e^{\alpha_2}p_0^{\alpha_2}\epsilon_{\alpha_20}\\ &+\sum_{k=1}^{D-1}(e^{\alpha_1}p_k^{\alpha_1}\epsilon_{\mu\alpha_1}+e^{\alpha_2}p_k^{\alpha_2}\epsilon_{\mu\alpha_2})\\ &=(e^{\alpha_1}p_0^{\alpha_1}-e^{\alpha_2}p_0^{\alpha_2})Q_{\gamma}^0+(e^{\alpha_1}p_1^{\alpha_1}-e^{\alpha_2}p_1^{\alpha_2})Y_{\gamma,1}^\mu\\ &+A_{\alpha_1\alpha_2}[e^\mu Q^\mu-e^\mu p_0^\mu Y_{\gamma,0}^\mu-e^\mu p_1^\mu Y_{\gamma,1}^\mu]\\ &+e^{\alpha_1}p_0^{\alpha_1}\epsilon_{\alpha_10}+e^{\alpha_2}p_0^{\alpha_2}\epsilon_{\alpha_20}\\ &+(e^{\alpha_1}-e^{\alpha_1}p_0^{\alpha_1})\epsilon_{\mu\alpha_1}+(e^{\alpha_2}-e^{\alpha_2}p_0^{\alpha_2})\epsilon_{\mu\alpha_2}\\ &\leq (e^{\alpha_1}p_0^{\alpha_1}-e^{\alpha_2}p_0^{\alpha_2}-A_{\alpha_1\alpha_2}e^\mu p_1^\mu)Q_{\gamma}^0\\ &+(e^{\alpha_1}p_1^{\alpha_1}-e^{\alpha_2}p_0^{\alpha_2}-A_{\alpha_1\alpha_2}e^\mu p_1^\mu)Y_{\gamma,1}^\mu\\ &+A_{\alpha_1\alpha_2}e^\mu Q_{\gamma}^\mu+A_{\alpha_1\alpha_2}e^\mu p_0^\mu\epsilon_{\mu0}+e^{\alpha_1}p_0^{\alpha_1}\epsilon_{\alpha_{10}}+e^{\alpha_2}p_0^{\alpha_2}\epsilon_{\alpha_{20}}\\ &+(e^{\alpha_1}-e^{\alpha_1}p_0^{\alpha_1})\epsilon_{\mu\alpha_1}+(e^{\alpha_2}-e^{\alpha_2}p_0^{\alpha_2})\epsilon_{\mu\alpha_2}\end{aligned} \tag{36}$$

where, in the first inequality, we use Eq. (13) repeatedly to write all yield terms either as a function of intensity μ or 0. Note that the left hand side of this inequality is a function of observable parameters. In the next two inequalities, we have written the right hand side as a function of $Y^{\mu}_{\gamma,1}$, the parameter we want to bound, as well as other observables and constants. Consequently, the lower bound of $Y^{\mu}_{\gamma,1}$ can be obtained as shown in Eq. (23).

For the parameters related to errors, the upper bounds are derived similarly. To derive $W_{y,1}^{\mu U}$, we can use the following

$$\begin{split} &e^{\alpha_1}Q_y^{\alpha_1}E_y^{\alpha_1} - e^{\alpha_2}Q_y^{\alpha_2}E^{\alpha_2} \\ &= &e^{\alpha_1}p_0^{\alpha_1}W_{y,0}^{\alpha_1} - e^{\alpha_2}p_0^{\alpha_2}W_{y,0}^{\alpha_2} + e^{\alpha_1}p_1^{\alpha_1}W_{y,1}^{\alpha_1} - e^{\alpha_2}p_1^{\alpha_2}W_{y,1}^{\alpha_2} \\ &+ \sum_{k=2}^{D-1}(e^{\alpha_1}p_k^{\alpha_1}W_{y,k}^{\alpha_1} - e^{\alpha_2}p_k^{\alpha_2}W_{y,k}^{\alpha_2}) \\ &\geq &(e^{\alpha_1}p_0^{\alpha_1} - e^{\alpha_2}p_0^{\alpha_2})W_{y,0}^0 - e^{\alpha_1}p_0^{\alpha_1}\epsilon_{\alpha_10} - e^{\alpha_2}p_0^{\alpha_2}\epsilon_{\alpha_20} \\ &+ (e^{\alpha_1}p_1^{\alpha_1} - e^{\alpha_2}p_1^{\alpha_2})W_{y,1}^{\mu} - e^{\alpha_1}p_1^{\alpha_1}\epsilon_{\mu\alpha_1} - e^{\alpha_2}p_1^{\alpha_2}\epsilon_{\mu\alpha_2} \\ &= &(e^{\alpha_1}p_0^{\alpha_1} - e^{\alpha_2}p_0^{\alpha_2})Q_y^0E_y^0 + (e^{\alpha_1}p_1^{\alpha_1} - e^{\alpha_2}p_1^{\alpha_2})W_{y,1}^{\mu} \\ &- e^{\alpha_1}p_0^{\alpha_1}\epsilon_{\alpha_10} - e^{\alpha_2}p_0^{\alpha_2}\epsilon_{\alpha_20} - e^{\alpha_1}p_1^{\alpha_1}\epsilon_{\mu\alpha_1} - e^{\alpha_2}p_1^{\alpha_2}\epsilon_{\mu\alpha_2}. \end{split}$$

Consequently, we can get an upper bound on $W_{y,1}^{\mu}$ as given by Eq. (25).

APPENDIX B ANALYTICAL MDI QKD BOUNDS

In this appendix, we derive Eq. (27) and Eq. (31) in the main text. We set $\alpha=\beta=\nu$ in analysis and use γ to represent either X or Y basis.

First, we can rewrite $Q_{\gamma}^{\alpha\beta}$ and $Q_{\gamma}^{\alpha\beta}E_{\gamma}^{\alpha\beta}$ as [10]

$$e^{\alpha+\beta}Q_{\gamma}^{\alpha\beta} = e^{\alpha+\beta} \sum_{k,l=0}^{D-1} p_k^{\alpha} p_l^{\beta} Y_{\gamma,kl}^{\alpha\beta},$$

$$e^{\alpha+\beta}Q_{\gamma}^{\alpha\beta} E_{\gamma}^{\alpha\beta} = e^{\alpha+\beta} \sum_{k,l=0}^{D-1} p_k^{\alpha} p_l^{\beta} e_{\gamma,kl}^{\beta} Y_{\gamma,kl}^{\alpha\beta}.$$
 (38)

In order to use other observables to bound $Y^{\mu\mu}_{\gamma,11},\,Q^{\alpha\beta}_{\gamma}$ can be expanded as follows:

$$e^{\alpha+\beta}Q_{\gamma}^{\alpha\beta}$$

$$=\sum_{k,l=0}^{D-1}e^{\alpha+\beta}p_{k}^{\alpha}p_{l}^{\beta}Y_{\gamma,kl}^{\alpha\beta}$$

$$=S_{1}+S_{2}+S_{3}+S(\alpha,\beta). \tag{39}$$

where

$$S_{1} = e^{\alpha+\beta} \sum_{l=0}^{D-1} p_{0}^{\alpha} p_{l}^{\beta} Y_{\gamma,0l}^{\alpha\beta},$$

$$S_{2} = e^{\alpha+\beta} (p_{1}^{\alpha} p_{0}^{\beta} Y_{\gamma,10}^{\alpha\beta} + \sum_{k=2}^{D-1} p_{k}^{\alpha} p_{0}^{\beta} Y_{\gamma,k0}^{\alpha\beta}),$$

$$S_{3} = e^{\alpha+\beta} p_{1}^{\alpha} p_{1}^{\beta} Y_{\gamma,11}^{\alpha\beta},$$

$$S(\alpha, \beta) = e^{\alpha+\beta} (\sum_{k=2}^{D-1} p_{k}^{\alpha} p_{1}^{\beta} Y_{\gamma,k1}^{\alpha\beta} + \sum_{l=2}^{D-1} p_{1}^{\alpha} p_{l}^{\beta} Y_{\gamma,1l}^{\alpha\beta})$$

$$+ \sum_{k=2}^{D-1} \sum_{l=2}^{D-1} p_{k}^{\alpha} p_{l}^{\beta} Y_{\gamma,kl}^{\alpha\beta}). \tag{46}$$

 S_1, S_2 and S_3 can be bounded separately as follows:

$$S_{1} \leq e^{\alpha+\beta} p_{0}^{\alpha} \sum_{l=0}^{D-1} p_{0}^{0} p_{l}^{\beta} (Y_{\gamma,0l}^{0\beta} + \epsilon_{\alpha 0}) = e^{\alpha+\beta} p_{0}^{\alpha} (Q_{\gamma}^{0\beta} + \epsilon_{\alpha 0}),$$

$$S_{2} = e^{\alpha+\beta} (\sum_{k=0}^{N-1} p_{k}^{\alpha} p_{0}^{\beta} Y_{\gamma,k0}^{\alpha\beta} - p_{0}^{\alpha} p_{0}^{\beta} Y_{\gamma,00}^{\alpha\beta})$$

$$\leq e^{\alpha+\beta} (p_{0}^{\beta} \sum_{k=0}^{D-1} p_{k}^{\alpha} (Y_{\gamma,k0}^{\alpha 0} + \epsilon_{\beta 0}) - p_{0}^{\alpha} p_{0}^{\beta} (Y_{\gamma,00}^{00} - \epsilon_{\alpha 0} - \epsilon_{\beta 0}))$$

$$= e^{\alpha+\beta} (p_{0}^{\beta} Q_{\gamma}^{\alpha 0} - p_{0}^{\alpha} p_{0}^{\beta} Q_{\gamma}^{00} + (p_{0}^{\beta} + p_{0}^{\alpha} p_{0}^{\beta}) \epsilon_{\beta 0} + p_{0}^{\alpha} p_{0}^{\beta} \epsilon_{\alpha 0}),$$

$$S_{3} \leq e^{\alpha+\beta} p_{1}^{\alpha} p_{1}^{\beta} (Y_{\gamma,11}^{\mu\mu} + \epsilon_{\alpha\mu} + \epsilon_{\beta\mu}). \tag{41}$$

The three inequalities in Eq. (41) are due to Eq. (19). Using Eq. (39) and Eq. (41), an upper bound on $Q_{\gamma}^{\alpha\beta}$ can be expressed as

$$e^{\alpha+\beta}Q_{\gamma}^{\alpha\beta}$$

$$\leq e^{\alpha+\beta}(p_{0}^{\alpha}Q_{\gamma}^{0\beta} + p_{0}^{\beta}Q_{\gamma}^{\alpha0} - p_{0}^{\alpha}p_{0}^{\beta}Q_{\gamma}^{00} + p_{1}^{\alpha}p_{1}^{\beta}Y_{\gamma,11}^{\mu\mu} + (p_{0}^{\alpha} + p_{0}^{\alpha}p_{0}^{\beta})\epsilon_{\alpha0} + (p_{0}^{\beta} + p_{0}^{\alpha}p_{0}^{\beta})\epsilon_{\beta0} + p_{1}^{\alpha}p_{1}^{\beta}(\epsilon_{\alpha\mu} + \epsilon_{\beta\mu})) + S(\alpha, \beta)$$

$$= T_{1} + e^{\alpha+\beta}p_{1}^{\alpha}p_{1}^{\beta}Y_{\gamma,11}^{\mu\mu} + S(\alpha, \beta) + \epsilon_{\bar{s}}, \tag{42}$$

where T_1 and $\epsilon_{\bar{s}}$ are defined in the main text.

Till now, $Q_{\gamma}^{\alpha\beta}$ has been almost replaced by a sum of other observables and parameters that can be calculated directly, except $Y_{\gamma,11}^{\mu\mu}$, which is the variable we need in the key rate formula, and $S(\alpha,\beta)$. Therefore, the next task is to bound $S(\alpha,\beta)$ with some observables to provide a bound for $Y_{\gamma,11}^{\mu\mu}$. Based on Eq. (19), we get a bound for $S(\alpha,\beta)$ as follows:

$$\leq e^{\alpha+\beta} \left(\sum_{k=2}^{D-1} p_{k}^{\alpha} p_{1}^{\beta} (Y_{\gamma,k1}^{\mu\mu} + \epsilon_{\alpha\mu} + \epsilon_{\beta\mu}) \right) \\
+ \sum_{l=2}^{D-1} p_{1}^{\alpha} p_{l}^{\beta} (Y_{\gamma,ll}^{\mu\mu} + \epsilon_{\alpha\mu} + \epsilon_{\beta\mu}) \\
+ \sum_{l=2}^{D-1} \sum_{l=2}^{D-1} p_{k}^{\alpha} p_{l}^{\beta} (Y_{\gamma,kl}^{\mu\mu} + \epsilon_{\alpha\mu} + \epsilon_{\beta\mu}) \\
+ \sum_{k=2}^{D-1} \sum_{l=2}^{D-1} p_{k}^{\alpha} p_{l}^{\beta} (Y_{\gamma,kl}^{\mu\mu} + \epsilon_{\alpha\mu} + \epsilon_{\beta\mu})) \\
\leq e^{2\mu} \left(A \sum_{k=2}^{D-1} p_{k}^{\mu} p_{1}^{\mu} Y_{\gamma,k1}^{\mu\mu} + B \sum_{l=2}^{D-1} p_{1}^{\mu} p_{l}^{\mu} Y_{\gamma,ll}^{\mu\mu} \right) \\
+ C \sum_{k=2}^{D-1} \sum_{l=2}^{D-1} p_{k}^{\mu} p_{l}^{\mu} Y_{\gamma,kl}^{\mu\mu}) + e^{\alpha+\beta} \left(\sum_{k=2}^{D-1} p_{k}^{\alpha} p_{1}^{\beta} (\epsilon_{\alpha\mu} + \epsilon_{\beta\mu}) \right) \\
+ \sum_{l=2}^{D-1} p_{1}^{\alpha} p_{l}^{\beta} (\epsilon_{\alpha\mu} + \epsilon_{\beta\mu}) + \sum_{k=2}^{D-1} \sum_{l=2}^{D-1} p_{k}^{\alpha} p_{l}^{\beta} (\epsilon_{\alpha\mu} + \epsilon_{\beta\mu})) \\
\leq G \cdot S(\mu, \mu) + \epsilon_{s} \\
\leq G e^{2\mu} (Q_{\gamma}^{\mu\mu} - p_{0}^{\mu} (Q_{\gamma}^{0\mu} + Q_{\gamma}^{\mu0}) + p_{0}^{\mu} p_{0}^{\mu} Q_{\gamma}^{00} \\
- p_{1}^{\mu} p_{1}^{\mu} Y_{\gamma,11}^{\mu\mu} + 2(p_{0}^{\mu} + p_{0}^{\mu} p_{0}^{\mu}) \epsilon_{\mu0}) + \epsilon_{s} \\
= G T_{s} - G e^{2\mu} p_{1}^{\mu} p_{1}^{\mu} Y_{\gamma,11}^{\mu\mu} + 2G e^{2\mu} (p_{0}^{\mu} + p_{0}^{\mu} p_{0}^{\mu}) \epsilon_{\mu0} + \epsilon_{s} \\
= G T_{s} - G e^{2\mu} p_{1}^{\mu} p_{1}^{\mu} Y_{\gamma,11}^{\mu\mu} + 2G \epsilon_{T_{s}} + \epsilon_{s}, \tag{43}$$

where all introduced constants are defined in the main text.

Finally, using Eq. (42) and Eq. (43), the lower bound of

 $Y^{\mu\mu}_{\gamma,11}$ is obtained in Eq. (27). In terms of $e^{p,\mu\mu}_{x,11}$ in the key rate formula, we first bound $e^{b,\mu\mu}_{y,11}$ based on $W^{\mu\mu}_{y,11}$. Similar to what we did in Eq. (42), we replace all the Q terms with QE terms, change the less than or equal sign to the greater than or equal sign, and change the signs of ϵ terms from plus signs to minus signs. Consequently, a lower bound on $Q_y^{\alpha\beta}E_y^{\alpha\beta}$ is given by

$$e^{\alpha+\beta}Q_{y}^{\alpha\beta}E_{y}^{\alpha\beta}$$

$$\geq e^{\alpha+\beta}(p_{0}^{\alpha}Q_{y}^{0\beta}E_{y}^{0\beta} + p_{0}^{\beta}Q_{y}^{\alpha0}E_{y}^{\alpha0} - p_{0}^{\alpha}p_{0}^{\beta}Q_{y}^{00}E_{y}^{00} + p_{1}^{\alpha}p_{1}^{\beta}W_{y,11}^{\mu\mu}$$

$$-(p_{0}^{\alpha} + p_{0}^{\alpha}p_{0}^{\beta})\epsilon_{\alpha0} - (p_{0}^{\beta} + p_{0}^{\alpha}p_{0}^{\beta})\epsilon_{\beta0}$$

$$-p_{1}^{\alpha}p_{1}^{\beta}(\epsilon_{\alpha\mu} + \epsilon_{\beta\mu})) + S(\alpha, \beta)$$

$$\geq T_{2} + e^{\alpha+\beta}p_{1}^{\alpha}p_{1}^{\beta}W_{y,11}^{\mu\mu} - \epsilon_{\bar{s}}, \tag{44}$$

using which the upper bound of $W_{u,11}^{\mu\mu}$ is obtained in Eq. (31).

REFERENCES

- [1] H.-K. Lo and H. F. Chau, "Unconditional security of quantum key distribution over arbitrarily long distances," Science, vol. 283, no. 5410, pp. 2050-2056, 1999.
- [2] P. W. Shor and J. Preskill, "Simple proof of security of the bb84 quantum key distribution protocol," Physical Review Letters, vol. 85, no. 2, p. 441,
- [3] L. Hoi-Kwong, M. Xiongfeng, and C. Kai, "Decoy state quantum key distribution," Physical Review Letters, vol. 94, no. 23, p. 230504, 2005.
- [4] C. Abellan, W. Amaya, M. Jofre, M. Curty, A. Acín, J. Capmany, V. Pruneri, and M. W. Mitchell, "Ultra-fast quantum randomness generation by accelerated phase diffusion in a pulsed laser diode," Optics Express, vol. 22, no. 2, pp. 1645-1654, 2014.
- [5] Z. Tang, Z. Liao, F. Xu, B. Qi, L. Qian, and H.-K. Lo, "Experimental demonstration of polarization encoding measurement-deviceindependent quantum key distribution," Physical Review Letters, vol. 112, no. 19, p. 190503, 2014.
- [6] N. K. Pathak, S. Chaudhary, Sangeeta, and B. Kanseri, "Phase encoded quantum key distribution up to 380 km in standard telecom grade fiber enabled by baseline error optimization," Scientific Reports, vol. 13, no. 1, p. 42445, 2023.
- [7] S. Nahar, T. Upadhyaya, and N. Lütkenhaus, "Imperfect phase randomization and generalized decoy-state quantum key distribution," Physical Review Applied, vol. 20, no. 6, p. 064031, 2023.
- [8] J. Yang, Z. Jiang, F. Benthin, J. Hanel, T. Fandrich, R. Joos, S. Bauer, S. Kolatschek, A. Hreibi, E. P. Rugeramigabo et al., "High-rate intercity quantum key distribution with a semiconductor single-photon source, Light: Science & Applications, vol. 13, no. 1, p. 150, 2024.
- [9] H.-W. Li, C.-M. Zhang, M.-S. Jiang, and Q.-Y. Cai, "Improving the performance of practical decoy-state quantum key distribution with advantage distillation technology," Communications Physics, vol. 5, no. 1, p. 231, 2022.
- [10] X. Ma, B. Qi, Y. Zhao, and H.-K. Lo, "Practical decoy state for quantum key distribution," Physical Review A-Atomic, Molecular, and Optical Physics, vol. 72, no. 1, p. 012326, 2005.
- [11] H.-K. Lo and J. Preskill, "Security of quantum key distribution using weak coherent states with nonrandom phases," arXiv preprint quantph/0610203, 2006.
- [12] B. Huttner, N. Imoto, N. Gisin, and T. Mor, "Quantum cryptography with coherent states," Physical Review A, vol. 51, no. 3, p. 1863, 1995.
- X.-B. Wang, "Beating the photon-number-splitting attack in practical quantum cryptography," Physical Review Letters, vol. 94, no. 23, p. 230503, 2005.
- [14] Y.-L. Tang, H.-L. Yin, X. Ma, C.-H. F. Fung, Y. Liu, H.-L. Yong, T.-Y. Chen, C.-Z. Peng, Z.-B. Chen, and J.-W. Pan, "Source attack of decoy-state quantum key distribution using phase information," Physical Review A-Atomic, Molecular, and Optical Physics, vol. 88, no. 2, p. 022308, 2013,
- [15] G. Currás-Lorenzo, K. Tamaki, and M. Curty, "Security of decoy-state quantum key distribution with imperfect phase randomization," IEICE Technical Report; IEICE Tech. Rep., 2022.

- [16] G. Currás-Lorenzo, S. Nahar, N. Lütkenhaus, K. Tamaki, and M. Curty, "Security of quantum key distribution with imperfect phase randomisation," Quantum Science and Technology, vol. 9, no. 1, p. 015025, 2023.
- [17] G. Chen, L. Wang, W. Li, Y. Zhao, S. Zhao, and J. Gruska, "Multiplepulse phase-matching quantum key distribution," Quantum Information Processing, vol. 19, no. 11, p. 416, 2020.
- [18] R.-Q. Wang, Z.-Q. Yin, X.-H. Jin, R. Wang, S. Wang, W. Chen, G.-C. Guo, and Z.-F. Han, "Finite-key analysis for quantum key distribution with discrete-phase randomization," Entropy, vol. 25, no. 2, p. 258, 2023.
- [19] Z. Tian, Z. Xie, Y. Chen, X. Fan, J. Huang, T. Mu, J. Guo, K. Wei, and S. Sun, "Reference-frame-independent quantum key distribution based on machine-learning-enhanced qubit-based synchronization," Science China Physics, Mechanics & Astronomy, vol. 68, no. 7, pp. 1-8, 2025.
- Z. Cao, Z. Zhang, H.-K. Lo, and X. Ma, "Discrete-phase-randomized coherent state source and its application in quantum key distribution," New Journal of Physics, vol. 17, no. 5, p. 053014, 2015.
- [21] S.-H. Sun, M. Gao, C.-Y. Li, and L.-M. Liang, "Practical decoy-state measurement-device-independent quantum key distribution," Physical Review A-Atomic, Molecular, and Optical Physics, vol. 87, no. 5, p. 052329, 2013.
- Z. Cao, "Discrete-phase-randomized measurement-device-independent quantum key distribution," Physical Review A, vol. 101, no. 6, p. 062325,
- [23] D. Tupkary, E. Y.-Z. Tan, S. Nahar, L. Kamin, and N. Lütkenhaus, "Qkd security proofs for decoy-state bb84: protocol variations, proof techniques, gaps and limitations," arXiv preprint arXiv:2502.10340, 2025.
- [24] X. Ma and M. Razavi, "Alternative schemes for measurement-deviceindependent quantum key distribution," Physical Review A, vol. 86, no. 6, p. 062319, 2012.
- [25] D. Gottesman, H.-K. Lo, N. Lutkenhaus, and J. Preskill, "Security of quantum key distribution with imperfect devices," in International Symposium onInformation Theory, 2004. ISIT 2004. Proceedings. IEEE, 2004, p. 136.
- [26] M. Koashi, "Simple security proof of quantum key distribution via uncertainty principle," arXiv preprint quant-ph/0505108, 2005.
- K. Tamaki, M. Koashi, and N. Imoto, "Unconditionally secure key distribution based on two nonorthogonal states," Physical Review Letters, vol. 90, no. 16, p. 167904, 2003.
- C. Gobby, a. Yuan, and A. Shields, "Quantum key distribution over 122 km of standard telecom fiber," Applied Physics Letters, vol. 84, no. 19, pp. 3762-3764, 2004.
- C. Panayi, M. Razavi, X. Ma, and N. Lütkenhaus, "Memory-assisted measurement-device-independent quantum key distribution," New Journal of Physics, vol. 16, no. 4, p. 043005, 2014.
- H.-K. Lo, M. Curty, and B. Qi, "Measurement-device-independent quantum key distribution," Physical Review Letters, vol. 108, no. 13, p. 130503, 2012.
- [31] X.-H. Jin, Z.-Q. Yin, S. Wang, W. Chen, G.-C. Guo, and Z.-F. Han, "Finite key analysis for discrete phase randomized bb84 protocol," Quantum Information Processing, vol. 23, no. 9, p. 312, 2024.
- [32] P. Zeng, H. Zhou, W. Wu, and X. Ma, "Mode-pairing quantum key distribution," Nature Communications, vol. 13, no. 1, p. 3903, 2022.
- M. Lucamarini, Z. L. Yuan, J. F. Dynes, and A. J. Shields, "Overcoming the rate-distance limit of quantum key distribution without quantum repeaters," Nature, vol. 557, no. 7705, pp. 400-403, 2018.